Journal of Contaminant Hydrology 182 (2015) 91–103

Contents lists available at ScienceDirect

Journal of Contaminant Hydrology

journal homepage: www.elsevier.com/locate/jconhyd

# Water and chloride transport in a fine-textured soil in a feedlot pen

Veizaga E.A. [a,b,*], Rodríguez L. [b], Ocampo C.J. [c]

[a] Consejo Nacional de Investigaciones Científicas y Técnicas (CONICET), Av. Rivadavia 1917 (C1033AAJ), Ciudad Autónoma de Buenos Aires, Argentina
[b] Centro de Estudios Hidroambientales (CENEHA), Facultad de Ingeniería y Ciencias Hídricas (FICH), Universidad Nacional del Litoral (UNL), Ciudad Universitaria, Ruta Nacional N° 168, Km 472,4. (3000), Santa Fe, Argentina
[c] School of Civil, Environmental and Mining Engineering, University of Western Australia, 35 Stirling Highway, 6009 Crawley, Western Australia, Australia

ARTICLE INFO

*Article history:*
Received 5 February 2015
Received in revised form 18 August 2015
Accepted 26 August 2015
Available online 29 August 2015

*Keywords:*
Feedlot pens
Clayed soils
Chloride transport
HYDRUS-1D
Atmospheric forcing

ABSTRACT

Cattle feeding in feedlot pens produces large amounts of manure and animal urine. Manure solutions resulting from surface runoff are composed of numerous chemical constituents whose leaching causes salinization of the soil profile. There is a relatively large number of studies on preferential flow characterization and modeling in clayed soils. However, research on water flow and solute transport derived from cattle feeding operations in fine-textured soils under naturally occurring precipitation events is less frequent. A field monitoring and modeling investigation was conducted at two plots on a fine-textured soil near a feedlot pen in Argentina to assess the potential of solute leaching into the soil profile. Soil pressure head and chloride concentration of the soil solution were used in combination with HYDRUS-1D numerical model to simulate water flow and chloride transport resorting to the concept of mobile/immobile—MIM water for solute transport. Pressure head sensors located at different depths registered a rapid response to precipitation suggesting the occurrence of preferential flow-paths for infiltrating water. Cracks and small fissures were documented at the field site where the % silt and % clay combined is around 94%. Chloride content increased with depth for various soil pressure head conditions, although a dilution process was observed as precipitation increased. The MIM approach improved numerical results at one of the tested sites where the development of cracks and macropores is likely, obtaining a more dynamic response in comparison with the advection–dispersion equation.



## 1. Introduction

Argentina's economy relies strongly on exports of agricultural and livestock production. Three decades ago, cattle grazing occurred almost exclusively on vast grasslands extending mainly in Argentinean Pampas region. However, during the nineties there was a remarkable agricultural transformation driven by the adoption of transgenic crops under the no-tillage system (Pengue, 2005). This transformation caused an increase of crop-covered land and the reduction of the land devoted to grazing, giving rise to feedlot activities. It is estimated that in 2009, 30% of all consumed and exported bovine meat came from feedlot establishments.

Cattle feeding in feedlot pens produces large amounts of manure and animal urine. Manure solutions resulting from surface runoff after precipitation events are composed of dissolved organic matter, nutrients, salts, antibiotics and

* Corresponding author at: Consejo Nacional de Investigaciones Científicas y Técnicas (CONICET), Av. Rivadavia 1917 (C1033AAJ), Ciudad Autónoma de Buenos Aires, Argentina.
*URL's:* eveizaga82@hotmail.com, e.veizaga@conicet.gov.ar (E.A. Veizaga).

http://dx.doi.org/10.1016/j.jconhyd.2015.08.009
0169-7722/

heavy metals, among other constituents (García et al., 2012). Early scientific contributions regarding feedlot activities focused on the potential impact on groundwater pollution by direct measurements of salt and nitrogen species concentration in water samples (Stewart et al., 1967; Mielke et al., 1970; Lorimor et al., 1972; Elliott et al., 1972; Smith et al., 1980). The studies conducted by Dormaar and Sommerfeldt (1986), Smith et al. (2001) and Olson et al. (2005) focused on nitrate groundwater pollution derived from manure application over agricultural soils. The environmental impact of livestock production has been extensively addressed for water and surface soil quality (Steinfeld et al., 2006). Nevertheless, the effect of manure solution leaching on the increase of salt content in the profile of fine-textured, highly productive soils has received less attention.

Fine-grained clay soils are prevalent in irrigation agriculture in many parts of the world. In vast extensions of the Argentinean Pampas, soils silt and clay fractions combined exceed 85%, being greater than 95% in some places (Castiglioni et al., 2005; Imhoff et al., 2010) resulting in highly productive soils due to their high nutrient content and water holding capacity. However, serious difficulties arise for solute transport assessment due to the combination of low saturated hydraulic conductivity, high bulk density, and the formation of desiccation cracks under unsaturated conditions (Chertkov and Ravina, 1998; Parker et al., 2001).

Feedlot operations in fine-textured soils introduce further complexity in the soil–water dynamics and the resulting solute transport that has not been extensively studied, especially in Argentina. Manure accumulation on the ground and livestock trampling lead to physical changes in the soil profile of feedlot pens. These changes, in turn, cause an increase in bulk density in the top horizons and constant soil moisture in the lower horizons (Mielke et al., 1974). This situation, as a result, modifies the dynamics of surface and subsurface water flow after precipitation events as large volumes of manure and animal urine are transported outside the pens into adjacent soil parcels via surface runoff (García et al., 2012). Those hydrological processes may be highly influenced by the soil clay content, prone to the presence of preferential flow paths due to alternating swelling/cracking in response to wetting/drying natural conditions.

Besides laboratory investigations and experimental plots, numerical modeling became a standard tool to assess the impact of agricultural/farm activities on soils and groundwater pollution. Hanson et al. (2006), Mantovi et al. (2006) and Crevoisier et al. (2008) have used numerical simulations to assess unsaturated flow and solute transport for chloride ($Cl^-$) and nitrogen under controlled irrigation regimes which provide a few examples of the above. Bouma (1981), Booltink and Bouma (1991), Greve et al. (2010) and Ventrella et al. (2000) have contributed to preferential flow characterization and modeling in fine-texture clayed soils under controlled irrigation conditions. These studies present some advantages by commonly reaching near saturation moisture conditions of the soil profile, thus facilitating monitoring activities and water sample collection. Instead of controlled water application conditions, Olson et al. (2005), Vaillant et al. (2009) and Miller et al. (2008) conducted field-scale experiments within feedlot premises or dairy farm premises (Baram et al., 2012a,b) under meteorological forcing. In Argentina, García et al. (2012) and Wyngaard et al. (2012) advanced in the chemical characterization of soil water on soil impacted by feedlot effluents without testing with modeling tools.

The randomness of precipitation events does not pose major difficulties in continuous data recording on the field scale. However, this can be challenging for in-situ soil water sampling. Some precipitation events, combined with low antecedent soil moisture, may not be enough to wet the soil profile favoring the migration of soil water into sample collection devices such as suction cup lysimeters. This is of particular relevance in fine-textured soils where soil moisture and solute transport in the profile are highly dependent on precipitation characteristics (Helling and Gish, 1991; Flury et al., 1994; Jacques et al., 2002). Baram et al. (2012a) demonstrated a large migration of nitrates in clayey soils under precipitation events due to preferential infiltration channels in a dairy farm enterprise. They also found that temporal variations in water content were largely associated with significant precipitation events.

This work investigates and documents the dynamics of water flow and leaching of a non-reactive solute through the unsaturated zone on a very fine-textured soil adjacent to a feedlot pen. The study site selected is located between a pen and a waste disposal lagoon representing transitional conditions. Water infiltration occurs under both natural precipitation conditions and water ponding conditions. Based on field data and numerical modeling, this work aims to address the following question: how do antecedent moisture and precipitation characteristics determine the migration of the non-reactive solute through the soil profile? HYDRUS-1D was used to simulate water flow and solute transport resorting to the concept of mobile/immobile water (MIM) for solute transport of $Cl^-$ concentration in order to represent preferential flow patterns that may develop on fine-textured soils.

## 2. Materials and methods

### 2.1. Study area

The study site corresponds to an active feedlot located 5 km north of San Justo city in the Province of Santa Fe, Argentina (Fig. 1). The feedlot has been in continuous operation for over the last 13 years, and it occupies 11.4 ha holding up to 9000 cattle in 33 pens. Pens are oriented east–west, each with a size of 40 m by 70 m.

The climate in the area is temperate, with an average annual precipitation of 1057 mm (Series 1920–2011, National Institute of Agricultural Technology — INTA). Winter months (June to August) are the driest, with 40% of the annual precipitation falling in the summer months (January to March). The minimum and maximum mean temperatures are 12 °C and 26 °C for the winter and summer season, respectively.

Feedlot activities take place on a transitional undulating land surface located between high flat areas of the landscape (average slope 0.05%) and flat lowland areas of the Salado River floodplain (Fig. 1). Soil characteristics across the area correlate well with geomorphological units of the landscape, from Typic Argiudoll on the Highland to Natracualf to the lowland areas of the Salado River floodplain (INTA, 1992).

Runoff washes pens surface producing a manure solution that is collected into surface channels near the

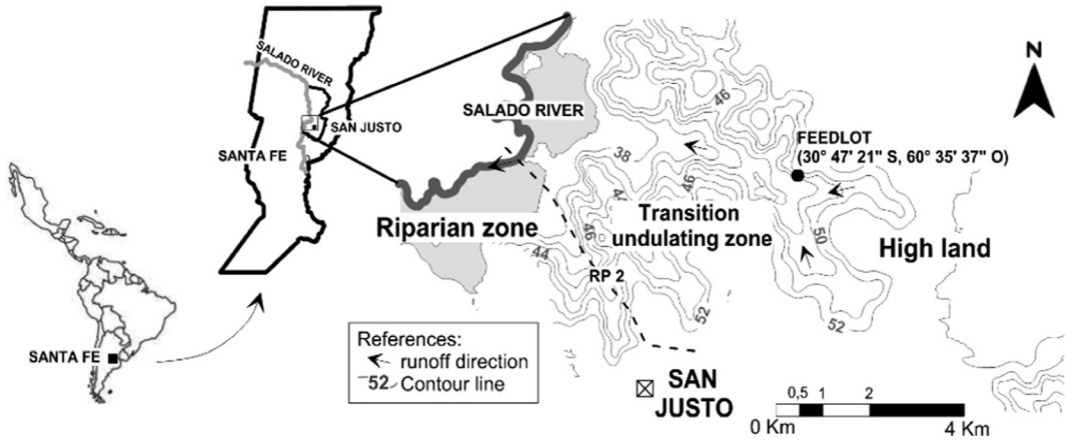


**Fig. 1.** San Justo city and feedlot establishment location. Geomorphological areas are also indicated to put the site location in a regional topographical/geographic context.

site. Then pen effluents are discharged into two waste disposal lagoons located at the lowest point within the feedlot premises (Fig. 2a, b). These effluent retention structures are deficiently managed, overflowing periodically spreading polluted water into down-gradient adjacent soils. The complexity of the surface water pathways and redistribution of manure during large precipitation events were taken into account for the experimental setting.

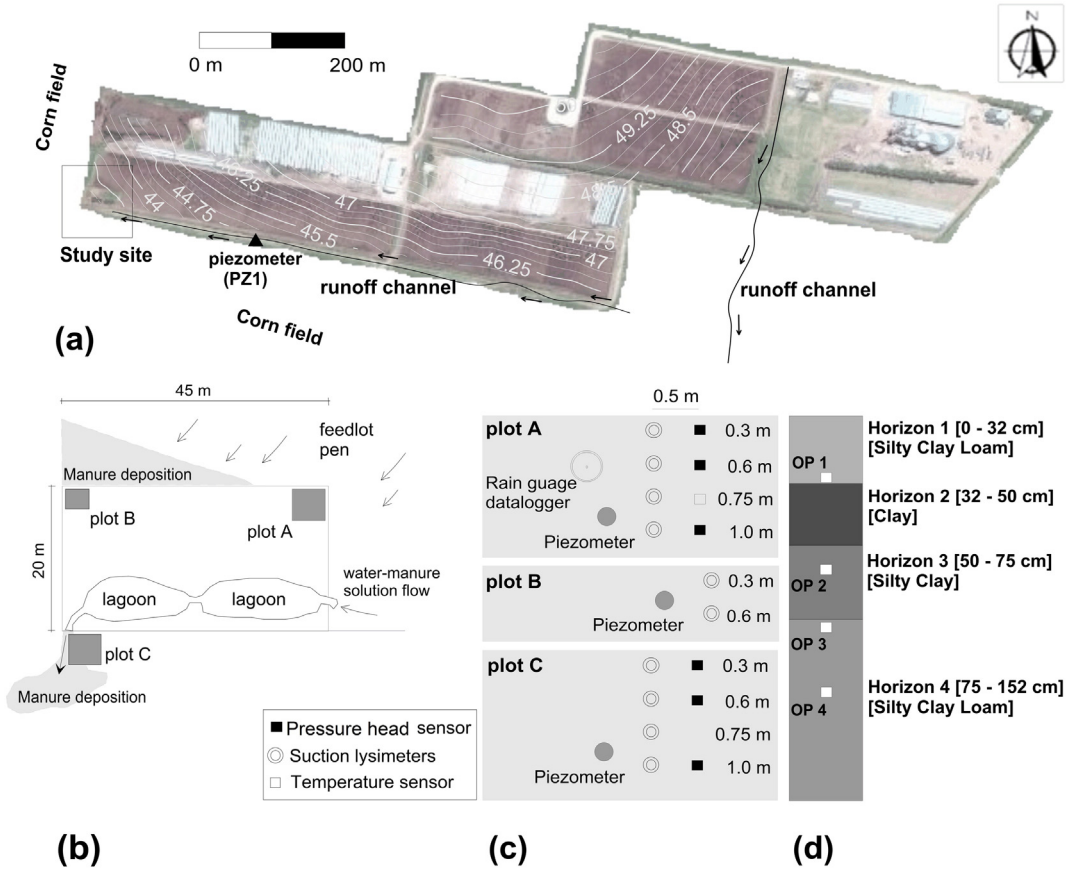


**Fig. 2.** (a) Topographic map of feedlot area (contour lines in m.a.s.l., contour interval: 0.25 m); (b) plan view of study site indicating instrumented plots A, B and C; (c) schematic plan view illustrating field monitoring equipment installed at each plot; (d) soil profile discretization, soil materials and location of observation nodes.

### 2.2. Experimental design, topographic and soil surveys

A detailed topographic survey of the feedlot area was conducted using a Leica® DGPS real-time kinematic (RTK) to identify the possible surface runoff pathways. Survey results also helped to choose the most suitable location for instrumentation and monitoring (Fig. 2a). Three locations were selected for water and solute transport monitoring, identified as plot A, plot B, and plot C in Fig. 2b. Plot A represents a well-developed soil profile showing vegetation growth on the surface. Due to its slightly higher topographic position, it remains under unsaturated conditions most of the time and is not frequently affected by runoff polluted waters unless the amount of precipitation surpasses 100 mm $d^{-1}$. Plot B is located at the lowest point of feedlot pens where manure solution accumulates after precipitation events, thus, representing a site directly affected by manure solution runoff. Ponding effluents nearby cause saturation conditions at this site for prolonged periods after precipitation events. Plot C is located down-gradient of the retention lagoons, presenting saturation conditions and overflow impact.

A 130 cm soil profile pit was excavated between plots A and B for soil horizons description and physical analyses. Disturbed soil samples were collected for particle size distribution testing by Bouyoucos method (Gee et al., 1986), and real density and porosity calculation following Soil Taxonomy protocols. Undisturbed soil samples were also collected from each horizon for bulk density determination.

### 2.3. Site instrumentation, field sampling and laboratory analyses

Plot A was instrumented first to gather data on soil water content and soil water chemistry distributions with depth. Pressure head sensors (Watermark®) were installed at 30, 60 and 100 cm depths, and a soil temperature sensor was placed at 10 cm depth. All sensors were wired to a data logger (Watchdog 400®) for automatic data collection at one-hour intervals. Soil water solution samples for physical and chemical analyses were collected via suction lysimeters (ceramic cups 0.5/1 bars, Soilmoisture Inc. US) placed at 30, 60, 75 and 100 cm depths. Only two suction cups were installed at plot B at depths of 30 and 60 cm. Shallow wells at both plots allowed monitoring the possible occurrence of a perched water table after precipitation events. Additionally, a water level sensor with logging capabilities was installed in a nearby 13 m deep piezometer (named PZ1 on Fig. 2a) to monitor groundwater level temporal variations. Plot C was instrumented with suction cups lysimeters at 30, 60, 75 and 100 cm depths. Fig. 2c depicts the instrumentation setup at each plot.

Precipitation was measured *in situ* with an automatic rain gauge installed at the site (Odyssey®). Other meteorological variables such as air temperature, relative humidity, atmospheric pressure, evaporation, wind speed and direction were obtained from a weather station located in San Justo city.

Manure is characterized by a high chloride—$Cl^-$ concentration in comparison with the soil solution $Cl^-$ concentration at the site, whereas its movement within the soil column is determined by water fluxes and meteorological forcing. As $Cl^-$ anion does not form complexes readily, it shows little adsorption to soil components and is not chemically altered by soil organisms. Consequently, these characteristics make $Cl^-$ a good tracer and indicator of sewage presence and manure contamination (Pratt et al., 1978; Bohn et al., 2002; Lockwood et al., 1995). Therefore, this non-reactive solute was used to analyze the influence of antecedent moisture conditions and precipitation characteristics on its migration through the soil profile.

All plots were monitored under natural conditions allowing the likely accumulation of manure on the surface after runoff episodes and vegetation growth.

Five 2, 3 and 4-day field campaigns were conducted between October 5, 2012, and April 12, 2013, for soil water solution collection during and after precipitation events. The sampling strategy was to cover a period transitioning from summer storms and hot temperatures to dry autumn season with sporadic low-precipitation events and cooler temperatures. In each field campaign, soil water solution samples were collected at 8 AM, 24 h after vacuum application to the cups, using a 60 ml syringe. Precipitation amount and antecedent soil moisture conditions posed serious limitations to the soil water solution extraction after prolonged dry periods. Hence, the sampling interval was defined by the time necessary to collect enough sample volume for laboratory analyses. In such a fine-textured soil, water could be extracted only when a soil threshold tension of around 75–85 kPa (−765/−867 cm) was achieved.

Soil solution electrical conductivity (EC) [μS $cm^{-1}$], temperature (T) [°C] and total dissolved solids (TDS) [mg $cm^{-3}$] were measured *in situ* using a multiparameter probe (90MLV-TPS®). $Cl^-$ concentration [mg $cm^{-3}$] was determined in the laboratory by the titrimetric method 4500-B (Clesceri et al., 1998).

### 2.4. Mathematical modeling

The HYDRUS-1D software package (Šimůnek et al., 2008), a standard numerical model for simulating water, heat, and solute movement in one-dimensional variably saturated porous media, was used as a tool to assist in the interpretation of monitored water and $Cl^-$ distribution at plots A and B. HYDRUS-1D numerically solves Richards' equation using linear finite element techniques and selected soil hydraulic properties models, which reads:

$$\frac{\partial \theta(h)}{\partial t} = \frac{\partial}{\partial z}\left[K(h)\ \frac{\partial h}{\partial z} - K(h)\right] - S(z,t) \quad (1)$$

where $\theta(h)$ is the volumetric water content [$L^3\ L^{-3}$], dependent on soil water potential expressed as pressure head $h$ [L] both varying in space and time, $z$ is the mean depth positive upward from the water table [L], $K(h)$ is the unsaturated hydraulic conductivity [$LT^{-1}$], $S(z,t)$ is a sink term representing water uptake by plant roots [$L^3\ L^{-3}\ T^{-1}$], and $t$ is the time [T]. The $S(z,t)$ term can be modeled with alternative formulations. In this work, Feddes et al. (1974) approach was selected. Parameters needed for its application are explained in the next section.

The model is capable of simulating layered porous media assuming either a vertical, horizontal or inclined direction for the flow domain. In this work, the ROSETTA Lite V1.1 model (Schaap et al., 2001) was used to determine initial estimates for the parameters of the water retention curve, adopting van

Genuchten's model for the $\theta(h)$ relationship (van Genuchten, 1980).

In a granular or single porosity media, the solute transport problem can be addressed by solving the advection–dispersion equation. Notwithstanding, the presence of aggregates or cracks may affect solutes movement, and their effect might be particularly pronounced on soils with high clay content causing deviations from single-porosity solute transport models. The fine-textured soil at the study site may be sensitive to preferential flow (Flury et al., 1994; Jarvis, 2007; Greve et al., 2010; Imhoff et al., 2010; Beven and Germann, 2013). Then, a non-equilibrium approach to simulate solute transport based on the concept of mobile-immobile (MIM) regions was chosen. The mobile (flowing) and immobile (stagnant) liquid pore regions for solute transport modeling equations are described by van Genuchten and Wierenga (1976):

$$\begin{aligned} &\theta = \theta_m + \theta_{im} \\ &\frac{\partial \theta_m c_m}{\partial t} + \frac{\partial \theta_{im} c_{im}}{\partial t} = \frac{\partial}{\partial z}\left(\theta_m D^w \frac{\partial c_m}{\partial z}\right) - \frac{\partial q c_m}{\partial z} \\ &\frac{\partial \theta_{im} c_{im}}{\partial t} = \omega(c_m - c_{im}) \end{aligned} \tag{2}$$

where $\Theta_m$ is the water content in the mobile region [$L^3\ L^{-3}$]; $\Theta_{im}$ is the water content in the immobile region [$L^3\ L^{-3}$], considered constant in this approach; ω is a first-order transfer rate [$T^{-1}$]; $c_m$ and $c_{im}$ are the $Cl^-$ concentrations in the mobile and immobile regions, respectively; $q$ is the volumetric flux density [$LT^{-1}$] and $D^w$ is the dispersion coefficient for the liquid phase [$L^2\ T^{-1}$]. The parameter $D^w$ is related to the longitudinal dispersivity, $D_L$ [L], the molecular diffusion $D_o$ and a tortuosity factor $\tau_W$ [−].

Bromide and salt transport modeling in sandy and fine-textured soils performed by van Dam et al. (1990) and Ventrella et al. (2000), respectively, were undertaken with the classical advection–dispersion equation. However, these studies showed substantial improvement in model performance when using the MIM water approach combined with the single porosity Richards' equation. A similar approach was adopted for this work.

## 3. Model implementation and parameters value estimates

Soil profile for the model implementation at plots A and B were represented by four layers after grouping similar horizons identified in the soil pit. Observation nodes were defined at 30, 60, 75 and 100 cm corresponding to the locations of pressure head sensors and suction cups lysimeters. Fig. 2b shows the soil profile discretization.

The simulated period extended for 190 days, from October 4, 2012 to April 12, 2013, encompassing both wetting and drying conditions. Since plot C was instrumented after this period, field and modeling results reported in this work are restricted to plots A and B.

Based on field data, initial values for $h$ at plot A were set as follows: −940 cm between 0 and 50 cm, −660 cm between 50 and 78 cm and −100 cm between 78 and 152 cm. At plot B, a linear variation from −50 cm on the soil surface up to 100 cm at the bottom of the profile was defined denoting saturation conditions.

Surface boundary conditions include daily precipitation and evaporation fluxes defined using meteorological data. The rain gauge data was integrated to obtain daily values, and the reference evapotranspiration rate ($ET_0$) was estimated using the Penman–Monteith equation (Allen et al., 2006). Fig. 3 presents the temporal distribution of both variables.

Two different bottom boundary conditions were used to model water movement through the soil profile as follows: a free drainage for plot A and a constant pressure head for plot B.

Height and root distribution of *Sorghum halepense*, the vegetation species grown at plot A, were monitored through the study period to provide HYDRUS-1D with key vegetation parameters. The estimated surface cover fraction (SCF), a HYDRUS-1D parameter, ranged from 0.5 to 0.8 for vegetation height values between 25 cm and 120 cm. These estimations were related to the leaf area index-LAI using the following equation:

$$LAI = -\frac{1}{a_i}\ln(1 - SCF) \tag{3}$$

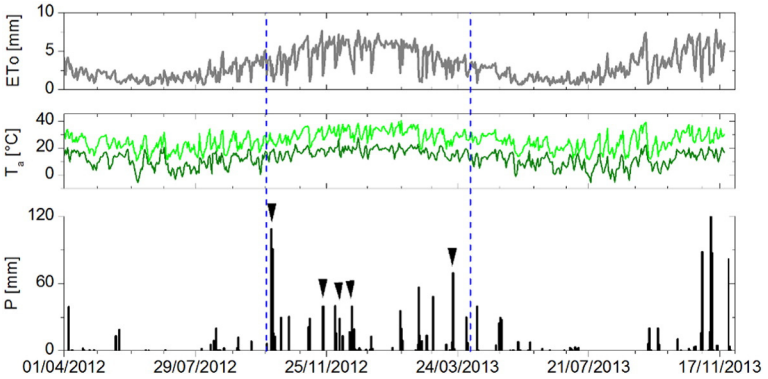


**Fig. 3.** Time series of meteorological variables. Above: daily reference evapotranspiration [$ET_0$] calculated by HYDRUS-1D. Center: maximum and minimum daily temperature. Below: daily precipitation registered at the study site. Arrows indicate the dates of soil water sampling campaigns. Dashed lines indicate the simulated period.

where $a_i$ is a constant for the radiation extinction by the canopy, adopted equal to 0.463. Due to frequent saturation conditions, almost no vegetation grew at plot B.

Abundant roots were found in the upper 25 cm at plot A, reducing significantly in depth at the beginning of the B horizon at 25 cm. Root distribution is introduced in HYDRUS-1D by means of Eq. (4):

$$S(h,z) = \alpha(h)b(z)T_p \tag{4}$$

where α(h) [−] is a stress function varying with $h$ between 0 and 1, b(z) [$L^{-1}$] represents a normalized water uptake distribution function and $T_p$ is the potential transpiration rate [$LT^{-1}$].

Finally, the initial and boundary conditions for the MIM solute transport model were set based on a combination of measured and reported data for the soil type identified at the study site. Initial $c_m$ was set equal to $Cl^-$ concentration of the first collected sample of the study period. Initial $c_{im}$ was set equal to the $Cl^-$ concentration reported by INTA for the predominant soil type in the area of San Justo (INTA, 1992). Transport boundary conditions were set equal to a variable concentration flux at the top and a zero concentration gradient at the bottom of the profile.

### 3.1. Model performance evaluation

Flow model performance was assessed quantitatively by means of classical statistical measures of goodness of fit (Zheng and Bennett, 2002) such as the mean error (ME), the mean absolute error (MAE) and the root mean square error (RMSE) between observed values ($O_i$) and model results ($E_i$) of $h$ values:

$$\mathrm{ME} = \frac{1}{n}\sum_{i=1}^{n}(O_i - E_i) * Wt_i \tag{5}$$

$$\mathrm{MAE} = \frac{1}{n}\sum_{i=1}^{n}|(O_i - E_i) * Wt_i| \tag{6}$$

$$\mathrm{RSME} = \sqrt{\frac{\sum_{i=1}^{n}[(O_i - E_i) * Wt_i]^2}{n-1}} \tag{7}$$

both $Oi$ and $Ei$ are associated with a weight factor $Wt_i$ that determines the representativeness of the observed data, assumed to be equal to one in this study.

## 4. Results and discussion

### 4.1. Soil type

The soil was classified as a Typic Argiudoll. Table 1 shows the seven horizons identified on the 152 cm soil pit.

It can be seen that the Bt horizon is characterized by a 13% increase in clay content, change relevant for water flow dynamics, root development, and dissolved solutes movement between the upper and lower layers. Despite this textural variation, porosity throughout the soil profile remained relatively constant, with a mean value of 0.40 (±1%) highlighting the presence of high silt content.

Bulk density increased with depth reflecting reduced organic matter, particle aggregation and root penetration on subsurface layers, which are also subject to the compacting weight of the soil above them (http://www.nrcs.usda.gov/Internet/FSE_DOCUMENTS/nrcs142p2_053256.pdf).

Compaction is particularly recognizable on the Bt1 and Bt2 horizons. This 47 cm thick layer has a strong to medium angular prism structure that desegregates in moderate to strong angular blocks. It also shows an abundance of slickensides, and it is extremely hard, firm, very plastic and adhesive. Moderate, thin root development occurs through cracks (Veizaga, 2015). These textural and structural characteristics explain the range of bulk density values determined by the cylinder method.

Ventrella et al. (2000) simulated flow and solute transport through a 210 cm fine-textured soil profile, with clay contents increasing with depth from 58.8% on the surface of the ground up to 77.2% at the bottom of the profile, values somehow similar to those at the study site. However, it is worth noting that Ventrella's soil is classified as Typic Epiaquerts whose genesis, structural and drainage characteristics are different from those of a Typic Argiudoll, which is the soil of the study site.

### 4.2. Climatic forcing and soil pressure head response

Before discussing numerical results, it is worth interpreting the physical behavior of soil water in response to atmospheric forcing given by precipitation and evapotranspiration. Fig. 4 shows pressure head at 30, 60 and 100 cm depths registered at

**Table 1**
Soil physical properties.

| | Soil layers — depth (cm) | | | | | | | | | |
|---|---|---|---|---|---|---|---|---|---|---|
| Soil horizon | Ao | Ap | Ap | Ap | Ap | B1 | Bt1 | Bt2 | B3 | C1 |
| Depth (cm) | 3–5 | 5–10 | 10–15 | 15–20 | 20–25 | 25–37 | 37–55 | 55–84 | 84–106 | 106–152 |
| % sand | 15.3 | 24 | 18.1 | 17.7 | 13.8 | 12.5 | 4.9 | 5.5 | 6.1 | 5.4 |
| % silt | 36.6 | 48.2 | 48.1 | 46.3 | 48.3 | 42.9 | 39.5 | 36.5 | 44.1 | 46.6 |
| % clay | 48.1 | 27.8 | 33.8 | 36 | 37.9 | 44.6 | 55.6 | 58 | 49.8 | 47.8 |
| $\rho_b$ (g $cm^{-3}$) | 0.65 | 1.07 | 1.27 | 1.57 | 1.37 | 1.46 | 1.54 | 1.58 | 1.5 | 1.44 |
| Porosity (e) | – | – | – | – | 0.43 | 0.39 | 0.4 | 0.38 | 0.41 | 0.4 |
| Real density (g $cm^{-3}$) | – | – | – | – | 2.56 | 2.47 | 2.55 | 2.54 | 2.56 | 2.4 |
| Texture (USDA) | C | CL | SCL | SCL | SCL | SC | C | C | SC | SC |

$\rho_b$: bulk density; SL: silt loam; SCL: silty clay loam; C: clay; SC: silty clay; CL: clay loam.

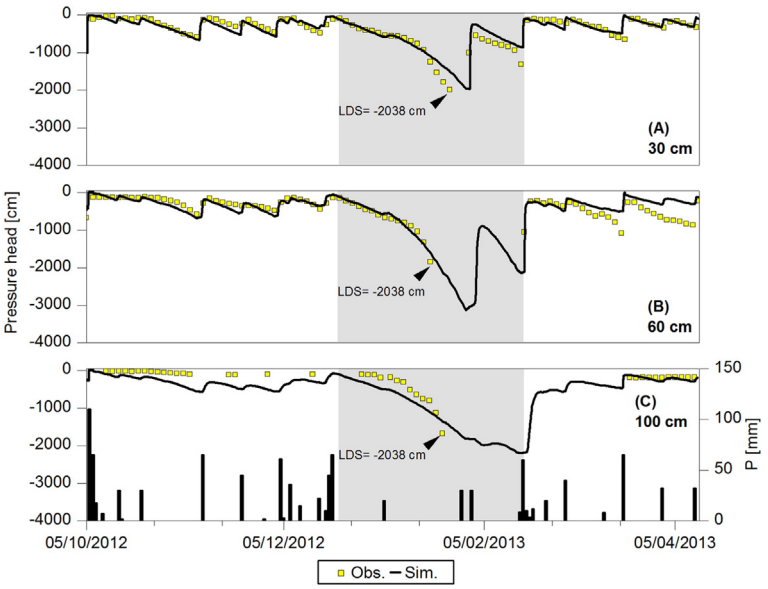


**Fig. 4.** Measured and simulated MP at depths of 30 cm (A), 60 cm (B) and 100 cm (C) at plot A.

plot A. Spatial and temporal patterns in response to particular precipitation events as well as to seasonal situations can be identified. The intensity of wetting and drying cycles varied with depth and time. At the beginning of the study period, the soil was nearly saturated at all depths until the end of December 2012. During this period, pressure head decreased/increased encompassing a series of precipitation events of various magnitudes. The intensity of drying and wetting cycles was similar at 30 and 60 cm whereas at 100 cm the signal showed little variability. During the warm summer months, pressure head increased significantly at all depths. The sensors reached the detection limit equal to −2000 cm (see the gray shaded area on Fig. 4). After this period, the soil rewetting behaved differently depending on depth, showing a delayed signal. Consecutive precipitation events caused a rapid rewetting first at 30 cm, and later at 60 cm, as indicated by field data in Fig. 4A and B. A higher accumulated precipitation amount was required to rewet deeper horizons.

These observations indicate that different precipitation amounts were needed to trigger distinct sensor reactions. A closer look at the pressure head response to individual precipitation events indicated that a precipitation threshold of around 40 mm needed to be overcome to allow downward flow beyond Bt1 horizon towards deeper horizons. This observation was also supported by the lack of response from the pressure head sensor located at the Bt2 horizon, which continued showing a drying trend in spite of the occurrence of precipitations of less than 40 mm (see Fig. 4B towards the end of the dry period). Besides, a rapid decrease in pressure head at 60 cm and 100 cm was observed after the hot summer. This change could be an indication of preferential flow paths for infiltrating water via cracks and small fissures. Alternatively, it may be the response to high soil moisture gradients or operational characteristics of the Watermark sensor (McCann et al., 1992) or a combination of these three causes. Among others, Flury et al. (1994) and Greve et al. (2010), conducted research on cracks formation and water dynamics on fine-textured soils.

Actually, the presence of superficial cracks was documented at the field site (Veizaga, 2015). On the one hand, Baram et al. (2012b) showed the continuity of cracks with depth on clayed soil, then one could think of a similar situation at the study site. On the other hand, Imhoff et al. (2010) investigated a Typic Argiudoll a few kilometers from the feedlot site. These authors described an increase in clay content with depth, associated with the formation of resistant blocks and prisms, favoring in turn the formation of cracks and fissures. These macropores would constitute the pores network in the sense referred to by Reynolds et al. (1995).

Observed flow patterns highlighted the key role of the Bt1 horizon in controlling vertical water flows that depend on antecedent soil moisture conditions, precipitation magnitude, and possible preferential flow paths. These observations on water dynamics were further investigated with the numerical model.

### *4.3. Soil water hydrochemical characterization: $Cl^-$ variability with depth*

Table 2 shows $Cl^-$ concentration and EC measured at plots A and B. Concentrations were also represented on box plot diagrams to facilitate results interpretation.

At plot A both, values of EC and $Cl^-$ concentration showed more dispersion in comparison with plot B, except at 30 cm. Plot B was frequently at near-saturation, providing more stable conditions in terms of flow. Contrary, plot A remained unsaturated most of the time affected by periodic wetting/drying cycles that influenced water and solute movement. EC at plot A never exceeded 2000 μS $cm^{-1}$ and experienced a slight increasing trend with depth while at plot B fluctuated between 1600 and 3000 μS $cm^{-1}$ during the study period, with a better defined trend with depth.

**Table 2**
Precipitation dates, precipitation amount—P, $Cl^-$ concentration and electrical conductivity—EC of the soil solution at plots A and B.

| Simulation day | Date | P [mm] | Measured concentrations | | | | | | |
|---|---|---|---|---|---|---|---|---|---|
| | | | $Cl^-$ 30 cm [mg $cm^{-3}$] | | $Cl^-$ 60 cm [mg $cm^{-3}$] | | $Cl^-$ 75 cm [mg $cm^{-3}$] | $Cl^-$ 100 cm [mg $cm^{-3}$] | |
| | | | EC 30 cm [μS $cm^{-1}$] | | EC 60 cm [μS $cm^{-1}$] | | EC 75 cm [μS $cm^{-1}$] | EC 100 cm [μS $cm^{-1}$] | |
| | | | Plot A | Plot B | Plot A | Plot B | Plot A | Plot A | Plot B |
| 1 | 05-Oct-12 | | | | | | | | |
| 2 | 06-Oct-12 | 108.6 | | | | | | | |
| 3 | 07-Oct-12 | 91.0 | | | | | | | |
| 4 | 08-Oct-12 | 15.9 | | | | | | | |
| 5 | 09-Oct-12 | 12.6 | | | | | | | |
| 6 | 10-Oct-12 | 0.3 | | | | | | | |
| 7 | 11-Oct-12 | | 0.036 | 0.048 | – | 0.120 | 0.076 | – | – |
| | | | (847) | (1629) | – | (2130) | (1345) | – | (2600) |
| 8 | 12-Oct-12 | | 0.036 | 0.064 | 0.060 | 0.170 | – | 0.155 | – |
| | | | (878) | (1562) | – | (2250) | – | – | (2700) |
| 9 | 13-Oct-12 | | 0.03 | 0.048 | 0.060 | 0.150 | 0.100 | 0.153 | 0.311 |
| | | | – | (1636) | – | (2260) | – | – | (2960) |
| 49 | 22-Nov-12 | 40 | | | | | | | |
| 50 | 23-Nov-12 | | 0.084 | 0.168 | 0.105 | 0.215 | 0.189 | 0.294 | 0.283 |
| | | | (1056) | (1987) | (1393) | (2340) | (1742) | (1950) | (1950) |
| 60 | 03-Dec-12 | 40.2 | | | | | | | |
| 61 | 04-Dec-12 | 15.8 | | | | | | | 0.283 |
| | | | | | | | | | (2360) |
| 62 | 05-Dec-12 | | 0.021 | 0.157 | 0.094 | 0.168 | 0.115 | 0.241 | 0.220 |
| | | | (773) | (2390) | (1580) | (2340) | (1299) | (2070) | (2380) |
| 63 | 06-Dec-12 | | 0.026 | 0.157 | – | 0.157 | – | 0.241 | – |
| | | | (747) | (2540) | – | (2340) | (1279) | (2010) | – |
| 75 | 18-Dec-12 | 40 | – | – | 0.021 | 0.189 | – | – | 0.314 |
| | | | – | – | (939) | (2240) | (712) | – | – |
| 76 | 19-Dec-12 | 14.4 | 0.042 | – | 0.042 | 0.147 | – | – | – |
| | | | (618) | (2290) | (1079) | (2440) | – | – | – |
| 77 | 20-Dec-12 | 19.4 | 0.021 | 0.063 | 0.042 | 0.157 | 0.052 | 0.094 | |
| | | | (624) | (2240) | (947) | (2540) | (677) | (1168) | |
| 78 | 21-Dec-12 | 1.5 | 0.021 | 0.094 | – | 0.126 | 0.052 | | – |
| | | | (654) | (1992) | (824) | (2291) | (702) | (1146) | – |
| 166 | 19-Mar-13 | 7.6 | | | | | | | |
| 167 | 20-Mar-13 | 69.6 | | | | | | | |
| 168 | 21-Mar-13 | 1.5 | 0.262 | 0.088 | 0.084 | 0.155 | – | – | – |
| | | | (1620) | (2090) | (993) | (2220) | – | – | – |
| 169 | 22-Mar-13 | | 0.251 | – | – | – | – | – | – |
| | | | (1670) | – | – | – | – | – | – |

On average, $Cl^-$ concentration increases with depth at both plots. At plot A, higher $Cl^-$ levels at 100 cm, where plant roots are virtually non-existing at 100 cm. Higher $Cl^-$ levels monitored at this depth would reflect that salt-concentrated water from the upper layers can reach lower layers through either the soil matrix and/or preferential flow paths. The highest $Cl^-$ concentration at 30 cm at plot A, equal to 0.26 mg $cm^{-3}$, was measured 15 days after the dry summer period was reversed by autumn precipitation events. It responds to a combination of high vegetation activity and evaporation from bare soil.

Plot B is frequently affected by ponded water–manure solution accumulated after precipitation events, becoming a relevant salt source. Its chemical characterization can help explain the occurrence of higher $Cl^-$ concentrations and EC since vegetation has no influence at this plot, suggesting the potential influence of lateral subsurface flows. This water showed important seasonal variability in agreement with the precipitation regime. Its EC ranged between 1710 μS $cm^{-1}$ and 7160 μS $cm^{-1}$ and its TDS between 860 mg $L^{-1}$ and 3730 mg $L^{-1}$. Eghball et al., (2002) measured manure EC highlighting its seasonal dependence, reporting values between 3800 and 5200 μS $cm^{-1}$. The observed dynamics of $Cl^-$ concentrations and its accumulation at depth are consistent with the findings by Olson et al. (2005). These authors reported $Cl^-$ accumulation up to 1.5 m depth under a cattle feedlot in Southern Alberta, Canada.

The $Cl^-$ distribution along the soil profile found at the feedlot highlighted the complex interaction between the physical processes governing the solute transport in the unsaturated zone for fine-textured soils under natural atmospheric forcing.

On the basis of field results, it can be suggested that the shallow Bt1 horizon did not constrain water and salt movement during and after high-precipitation events. Moreover, the accumulation of salt in depth could be controlled by the vertical water balance between precipitation and evapotranspiration during times of scarce rains and the development of cracks in the soil layers.

### 4.4. Simulated water flow patterns

Water flow and $Cl^-$ distribution along the soil profile were further investigated by the use of numerical modeling. Model parameters for water flow were first calibrated for plot A and then used to explore flow conditions and $Cl^-$ distribution at plot B. Four layers were considered adequate for a reasonable numerical representation of water and solute movement (Fig. 2d).

HYDRUS-1D simulations assumed single porosity van Genuchten–Mualem hydraulic property relationships. Based on the textural characteristics for each horizon, saturated water content $\theta_s$, residual water content $\theta_r$, inverse of the air entry value $\alpha$, pore size distribution index $n$, saturated hydraulic conductivity $K_s$ and pore connectivity parameter $l$ were initially estimated by means of the model ROSETTA Lite Version 1.1, available in HYDRUS-1D (Schaap et al., 2001).

In Rosetta, the retention curve as well as the hydraulic conductivity curve, are constructed with hundreds of soil samples extracted from agricultural and non-agricultural soils of the northern hemisphere (Schaap and Leij, 1998a,b). Therefore, their representativeness for Argentinean soils may be questioned. For that matter, initial parameter values were later adjusted during the calibration process using HYDRUS-1D inverse routine taking into account published parameter values for the study area (Imhoff et al., 2010).

The simulation period covered 190 days from October 5, 2012 until April 12, 2013. Calibrated soil hydraulic parameters for each model layer are presented in Table 3. Parameter values reflect the textural contrast between the Ap/B1 and Bt horizons. Even though each parameter has a well-defined physical meaning, van Genuchten and Nielsen (1985) warned that some of them, such as $\alpha$ and $\theta_r$ may be of empirical character. Despite this observation, the value of $\alpha$ reduced by half from 0.0063 to 0.0036 for lower layers in agreement with higher clay contents and, therefore, higher air entry values. The $K_s$ parameter was adjusted to 30.6 cm $d^{-1}$ for the top layer and reduced to one-third of that value for lower layers. For a Typic Argiudoll of the San Justo Group, with textural characteristics similar to those determined at the study site, Imhoff et al. (2010) reported a saturated hydraulic conductivity of 168 cm $d^{-1}$ for a no-till, wheat/soybean sequence soil use.

As shown in Fig. 4, there is a good agreement between simulated and observed pressure head at different depths at plot A. Simulated $h$ promptly responded to precipitation events of different magnitude and correctly captured near saturation conditions registered by all three sensors prior to the beginning of the dry period. Model performance indicators are summarized in Table 4. Deviations between observed and simulated pressure head can be attributed to different causes, among them: field measurements errors, model input and model structure errors, or their combination. RMSE values resulted similar at 30 and 60 cm, indicating that the model replicates observed pressure head reasonably well. However, an increase in RMSE values, and also in ME and MAE, occurred at 100 cm where the model performance decreased from the beginning to the end of the simulation period. It is worth noting that the number of data points available at 100 cm was reduced by more than half. ME was always positive indicating that simulated results slightly underestimate observed values.

**Table 4**
Model goodness-of-fit estimators for pressure head at plot A.

| Depth (cm) | Number of observation | ME | MAE | RMSE |
|---|---|---|---|---|
| 30 | 186 | −0.0024 | 0.0146 | 0.0226 |
| 60 | 163 | −0.0058 | 0.0207 | 0.0327 |
| 100 | 83 | 0.0259 | 0.0287 | 0.0340 |

At this point it is worth discussing whether the use of 1D-simple porosity–permeability model (SPM) is justified in soils prone to develop preferential flow via cracks where the dual-porosity model (DPM) may be more suitable. The choice of the SPM approach was based on constraints and difficulties in obtaining separated flow measurements for slow (matrix) and fast (preferential flow) regions at field scale required to validate a DPM model. Pressure head sensors measure bulk soil moisture, i.e. moisture contributed by mobile and immobile water alike, in proportions that will depend on the soil moisture condition. For instance, one could speculate that if the sensor is located at or near a crack formed after a drying period, it would measure mobile water after the first rain. If the soil moistens enough so as to close small cracks, then the sensor would measure predominantly immobile water. As presented in Köhne et al. (2009), the acceptable SPM performance achieved here with meaningful physical soil parameters has been reported in previous studies. These authors also highlighted the limitation in using flow data alone for the identification of DPM's parameter and the role of preferential flow in structured soils. The potential role of preferential flow (e.g. cracks) is later discussed using $Cl^-$ transport modeling with a MIM approach.

### 4.5. Simulated chloride dynamics

Both modeling approaches available in HYDRUS-1D for $Cl^-$ transport were used and compared prior to assisting in the interpretation of the field data. Fig. 6 shows the $Cl^-$ concentrations observed at depths of 30, 60, 75 and 100 cm at plot A, and model results obtained from the advection–dispersion transport equation—ADE and the mobile–immobile solute transport—MIM. Concentration values measured at plot B

**Table 3**
Fitted soil hydraulic parameters for modeled horizons.

| Parameter | 1° layer (SCL) (0–32 cm) | 2° layer (C) (32–50 cm) | 3° layer (SC) (50–74 cm) | 4° layer (SCL) (74–152 cm) |
|---|---|---|---|---|
| $\theta_r$ ($cm^3$ $cm^{-3}$) | 0.089 | 0.200 | 0.195 | 0.192 |
| $\theta_s$ ($cm^3$ $cm^{-3}$) | 0.412 | 0.400 | 0.380 | 0.400 |
| $\alpha$ ($cm^{-1}$) | 0.0063 | 0.0036 | 0.0045 | 0.0050 |
| $n$ (−) | 1.53 | 1.14 | 1.22 | 1.23 |
| $K_s$ (cm $d^{-1}$) | 30.60 | 10.83 | 10.80 | 10.82 |
| $l$ (−) | 5 | 5 | 0.5 | 0.5 |

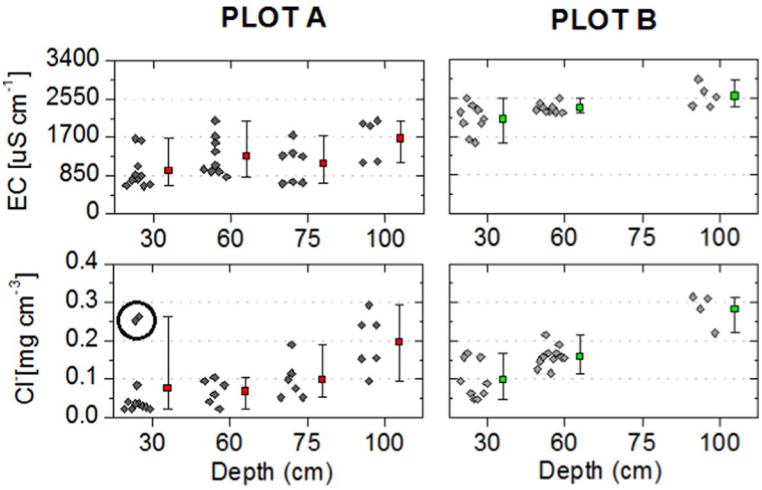


**Fig. 5.** $Cl^-$ concentration and EC at different depths.

were also included to explain similar/dissimilar patterns at both sites.

Results showed that model predictions agree reasonably well with field data at different depths, particularly for the upper soil layers. Adopting the MIM approach improved numerical results at plot A, where a combination of the soil matrix and preferential flow was documented and simulated. A more dynamic response was obtained in comparison with the ADE approach that underestimated measured concentrations at all depths in plot A for a wide range of values. This result is consistent with $Cl^-$ transport modeling and bromide breakthrough curve simulations results on fine-textured soils

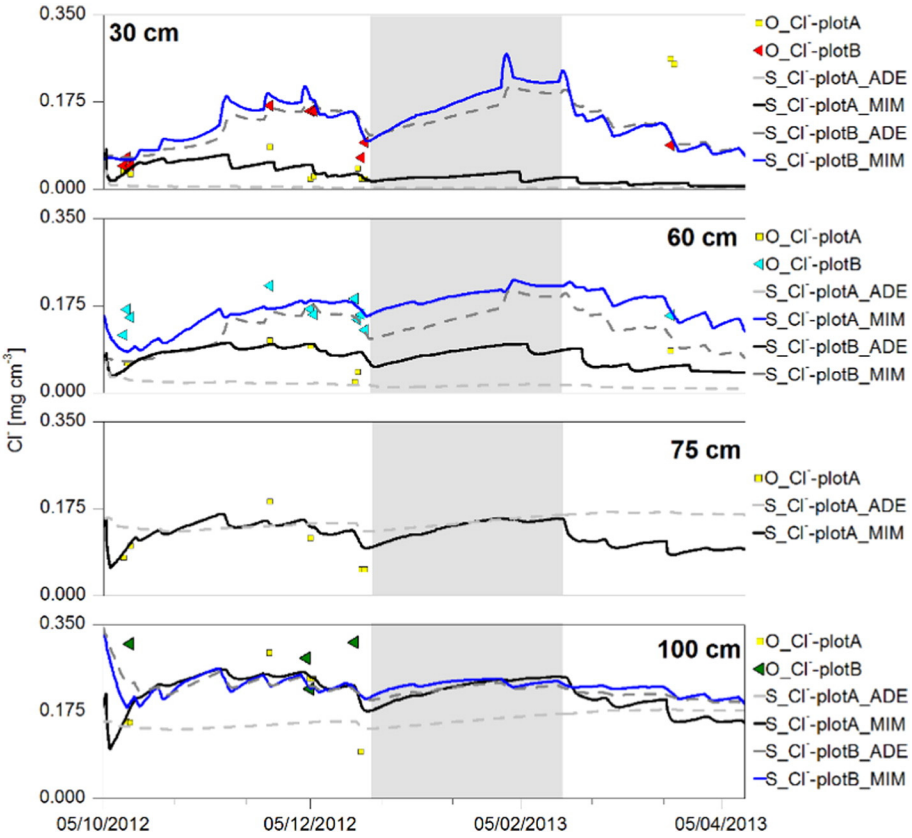


**Fig. 6.** Comparison between simulated (lines) and measured (symbols) $Cl^-$ concentration at depths of 30, 60, 75 and 100 cm at plots A and B. Solid lines correspond to MIM method and dashed lines correspond to ADE method. Shaded gray area represents dry period.

reported by Ventrella et al. (2000), Jacques et al. (2002) and Simůnek et al. (2003). All these authors found a better performance of the MIM approach over the ADE approach.

The model underestimated the $Cl^-$ concentration measured after the dry period at 30 cm at plot A, probably caused by salt concentration. The measured value almost tripled the $Cl^-$ levels of previous campaigns (see circled points in Fig. 5).

At plot B, differences between modeling results obtained with the two approaches tested are less distinguishable. At plot B ponded manure solution nearby may help maintain near-saturation conditions. In comparison with plot A where wetting/drying cycles had a more prominent effect on water flow and solute transport, preferential flow paths were not likely to form at this site, and vegetation growth was very limited. At plot B, the model predicted the increase in $Cl^-$ concentrations at 30 and 60 cm during the dry season with concentration values comparable with field measurements.

The contrast with model responses for the ADE and MIM approaches also highlighted the importance of the mechanism for $Cl^-$ delivery to the soil surface and the degree of equilibrium conditions in concentration values between immobile and mobile zones across the soil profile. Following Köhne et al. (2009) discussion on the topic, the MIM approach was adequate for plot A, where possible structural control may result in non-equilibrium conditions between MIM zones. At this site, $Cl^-$ was applied as a pulse input from occasional pen runoff after precipitation events. Surface condition differed from that at plot B where a continuous supply of water and $Cl^-$ resulted in $Cl^-$ concentrations at equilibrium between MIM zones. These observations also emphasize the importance of properly selecting a monitoring site to characterize a given phenomenon due to the number of processes involved.

Calibrated $Cl^-$ transport model parameters are presented in Table 5. Due to the inability to measure transport parameters or to rely on published values for similar soils for comparison purposes, calibrated parameter values are uncertain. Also, it is recognized that the multiple parameters combinations can lead to a non-unique result. Consequently, a sensitivity analysis was performed to ascertain the model response to certain parameters. If one considers $\theta_{im}$, $\omega$, $D_L$ and $D_o$ for each layer, the number of parameters candidates to be tested totals 16. Based on numerous testing, and to simplify the analysis, only parameters of model layer 2 were modified one at a time with respect to their calibrated value.

Numerical results were evaluated by computing ME, MAE, and RMSE for all layers collectively. Here, calibrated concentrations were considered as observed values. Table 6 shows the set of simulations and parameters values selected for the analysis.

Tested diffusion coefficient values for $Cl^-$ ($D_o$) were extracted from the literature (Rowell et al., 1967; van Rees et al., 1991).

**Table 6**
Set of sensitivity runs for transport parameters of model layer 2.

| Parameter | ME | MAE | RSME |
|---|---|---|---|
| $D_L = 10$ cm | 0.02508 | 0.05227 | 0.1311 |
| $D_L = 20$ cm | 0.02537 | 0.05204 | 0.1308 |
| $D_L = 30$ cm | 0.02554 | 0.05195 | 0.1306 |
| $\theta_{im} = 0.05$ | 0.03986 | 0.05199 | 0.1372 |
| $\theta_{im} = 0.1$ | 0.02508 | 0.05227 | 0.1311 |
| $\theta_{im} = 0.2$ | −0.00445 | 0.03714 | 0.0747 |
| $\omega = 0.008$ | 0.02441 | 0.05256 | 0.1319 |
| $\omega = 0.016$ | 0.02508 | 0.05227 | 0.1311 |
| $\omega = 0.04$ | 0.02579 | 0.05192 | 0.1300 |
| $D_o = 0.017$ | 0.02513 | 0.05229 | 0.1311 |
| $D_o = 0.7$ | 0.02512 | 0.05228 | 0.1311 |
| $D_o = 1.7$ | 0.02508 | 0.05227 | 0.1311 |

Selected values were equal to 0.17, 0.77 and 1.7 $cm^2\ d^{-1}$, obtaining no significant changes in model results. Similarly, the default value for the longitudinal dispersivity ($D_L$) suggested by HYDRUS-1D, equal to 10 cm, was the calibrated value. Using longitudinal dispersivities of 20 and 30 cm did not modify model results substantially.

Following a similar approach to that of Ventrella et al.'s (2000), $\theta_{im}$ and the mass transfer rate $\omega$ were selected as calibration parameters and later evaluated through the sensitivity analysis. The model was not very sensitive to the value of the transfer rate $\omega$. However, it was sensitive to the value of $\theta_{im}$. This analysis showed the model dependency on immobile water availability to reproduce adequately observed $Cl^-$ concentrations. This dependency also supports the use of the MIM approach for solute transport in the soil studied. However, the differences between simulated and observed $Cl^-$ concentrations at 30 cm in certain extreme cases could be attributed to the input of water with high salt concentration.

## 5. Conclusions

A 190 day field experiment was conducted at two sites, A and B, in order to address the dynamics of water flow and leaching of a non-reactive solute through the unsaturated zone on a very fine-texture soil near a feedlot pen, where infiltrating water occurs under natural precipitation and soil surface ponding conditions.

The results from this study showed that $Cl^-$ levels increased with depth in the soil profile in agreement with some previous research that identified its source in the first soils horizons due to $Cl^-$ accumulation from feedlot activities and root water uptake. Surface runoff from pens after precipitation events directly contributed to the redistribution of $Cl^-$ which is infiltrated using both soil matrix and preferential flow domains, the later becoming important upon precipitation magnitude and cracks development, further after dry temporal periods.

**Table 5**
Solute transport parameters.

| Parameter | 1° layer (SCL) (0–32 cm) | 2° layer (C) (32–50 cm) | 3° layer (SC) (50–74 cm) | 4° layer (SCL) (74–152 cm) |
|---|---|---|---|---|
| $\rho_b$ ($g\ cm^{-3}$) | 1.23 | 1.52 | 1.58 | 1.44 |
| $D_L$ (cm) | 10 | 10 | 10 | 10 |
| $D_o$ ($cm^2\ d^{-1}$) | 1.7 | 1.7 | 1.7 | 1.7 |
| $\theta_{im}$ ($cm^3\ cm^{-3}$) | 0.1 | 0.2 | 0.2 | 0.2 |
| $\omega$ ($d^{-1}$) | 0.016 | 0.016 | 0.016 | 0.016 |

$\rho_b$ = bulk density; $D_L$ = longitudinal dispersivity; $D_o$ = molecular diffusion coefficient; $\theta_{im}$ = immobile water content; $\varpi$ = mass transfer rate coefficient.

The study has contributed to further understanding water and $Cl^-$ movement in a layered soil with the presence of a shallow heavy-clayed layer such as the Bt1 horizon, previously believed to act as a strong flow barrier impeding the transport of pollutants from the surface layers towards the groundwater. It was shown that downward transport of $Cl^-$ was effective for large precipitation events.

Results also highlighted the need for a good characterization of the surface water dynamics and its chemical composition from feedlot pens as they impacted on the $Cl^-$ distribution with depth. Plot B always showed higher $Cl^-$ concentrations for all depths at the site due to manure accumulation in the soil surface layers from pens runoff. Plot A was affected by runoff from pens with $Cl^-$ input as a pulse (comparable to leaching tests), the resulting $Cl^-$ levels trend with depth obtained under natural precipitation conditions were opposed to observations reported by recent studies from leaching tests showing declining concentrations with depth and time.

Results from the combined use of the SPM for water flow and the MIM approach for $Cl^-$ transport have helped identify the relative importance of preferential flow in two feedlot pen plots subject to different surface water dynamics and $Cl^-$ inputs. Adopting the MIM approach improved numerical results at plot A, where cracks and macropores may have developed, obtaining a more dynamic response in comparison with the ADE approach. No significant differences in modeling results were obtained at plot B using the ADE and the MIM approaches. This result may be due to the fact that at that site frequent ponding conditions produced more stable values of soil pressure head, being the MIM solute transport not appropriate in such a case. In addition, the existence of lateral subsurface flows is possible.

## Acknowledgments

The authors would like to thank the staff of “Los Niños” feedlot establishment for allowing the development of this research, and the Ministerio de Ciencia e Innovación Productiva (MINCyT) (PFIP 2008-1. 2011/2012), Universidad Nacional del Litoral (UNL) (C.A.I.+D 2011, 50120110100261), and Consejo Nacional de Investigaciones Científicas y Técnicas (CONICET) for their partial financial support. The authors are also grateful to the anonymous reviewer whose comments and suggestions helped to enhance the quality of this work.

## References

Allen, R., Pereira, L., Raes, D., Smith, M., 2006. Evapotranspiración del cultivo. Guías para la determinación de los requerimientos de agua de los cultivos. Estudio FAO riego y drenaje N° 56. Organización de las Naciones Unidas para la agricultura y la alimentación. Roma (326 pp.).

Baram, S., Arnon, S., Ronen, Z., Kurtzman, D., Dahan, O., 2012a. Infiltration mechanism controls nitrification and denitrification processes under dairy waste lagoon. J. Environ. Qual. 41 (5), 1623–1632.

Baram, S., Kurtzman, D., Dahan, O., 2012b. Water percolation through a clayed vadose zone. J. Hydrol. 424, 165–171.

Beven, K.J., Germann, P.F., 2013. Macropores and water flow in soils revisited. Water Resour. Res. 49, 3071–3092.

Bohn, H.L., Myer, R.A., O'Connor, G.A., 2002. Soil Chemistry. John Wiley & Sons, New York.

Booltink, H.W.G., Bouma, J., 1991. Physical and morphological characterization of bypass flow in a well-structured clay soil. Soil Sci. Soc. Am. J. 55 (5), 1249–1254.

Bouma, J., 1981. Field measurement of soil hydraulic properties characterizing water movement through swelling clay soils. J. Hydrol. 45, 149–158.

Castiglioni, M.G., Morrás, H.J.M., Santanatoglia, O.J., Altinier, M.V., 2005. Shrinkage of soil aggregates from rolling pampa argiudolls differentiated by their clay mineralogy. Ci Suelo (Argentina) 23 (1), 13–22.

Chertkov, V.Y., Ravina, I., 1998. Modeling the crack network of swelling clay soils. Soil Sci. Soc. Am. J. 62 (5), 1162–1171.

Clesceri, L.S., Greenberg, A.E., Eaton, A.E., 1998. Standard Methods for the Examination of Water and Wastewater. American Public Health Association, Washington, DC (ed. 20).

Crevoisier, D., Popova, Z., Mailhol, J.C., Ruelle, P., 2008. Assessment and simulation of water and nitrogen transfer under furrow irrigation. Agric. Water Manag. 95 (4), 354–366.

Dormaar, J.F., Sommerfeldt, T.G., 1986. Effect of excess feedlot manure on chemical constituents of soil under nonirrigated and irrigated management. Can. J. Soil Sci. 66 (2), 303–313.

Eghball, B., Wienhold, B.J., Gilley, J.E., Eigenberg, R.A., 2002. Mineralization of manure nutrients. J. Soil Water Conserv. 57 (6), 470–473.

Elliott, L.F., McCalla, T.M., Mielke, L.N., Travis, T.A., 1972. Ammonium, nitrate, and total nitrogen in the soil water of feedlot and field soil profiles. Appl. Microbiol. 23 (4), 810–813.

Feddes, R.A., Bresler, E., Neuman, S.P., 1974. Field test of a modified numerical model for water uptake by root systems. Water Resour. Res. 10 (6), 1199–1206.

Flury, M., Flühler, H., Jury, W.A., Leuenberger, J., 1994. Susceptibility of soils to preferential flow of water: a field study. Water Resour. Res. 30 (7), 1945–1954.

García, A.R., Maisonnave, R., Massobrio, M.J., de Iorio, F., Alicia, R., 2012. Field-scale evaluation of water fluxes and manure solution leaching in feedlot pen soils. J. Environ. Qual. 41 (5), 1591–1599.

Gee, G.W., Bauder, J.W., Klute, A., 1986. Particle-size analysis. Methods of soil analysis. Part 1. Physical and Mineralogical Methods, pp. 383–411.

Greve, A., Andersen, M.S., Acworth, R.I., 2010. Investigations of soil cracking and preferential flow in a weighing lysimeter filled with cracking clay soil. J. Hydrol. 393 (1), 105–113.

Hanson, B.R., Simůnek, J., Hopmans, J.W., 2006. Evaluation of urea–ammonium–nitrate fertigation with drip irrigation using numerical modeling. Agric. Water Manag. 86 (1), 102–113.

Helling, C.S., Gish, T.J., 1991. Physical and chemical processes affecting preferential flow. In: Gish, T.J., Shirmohammadi, A. (Eds.), Preferential flow. Proc. Natl. Symp. Am. Soc. Agric. Engr.St. Joseph, MI., Chicago, IL., pp. 77–86

Imhoff, S., Ghiberto, P.J., Grioni, A., Gay, J.P., 2010. Porosity characterization of Argiudolls under different management systems in the Argentine Flat Pampa. Geoderma 158 (3), 268–274.

INTA, 1992. Soil Maps of Argentine Republic, Sheet 3160-14-San Justo.

Jacques, D., Simůnek, J., Timmerman, A., Feyen, J., 2002. Calibration of Richards' and convection–dispersion equations to field-scale water flow and solute transport under rainfall conditions. J. Hydrol. 259 (1), 15–31.

Jarvis, N.J., 2007. A review of non-equilibrium water flow and solute transport in soil macropores: principles, controlling factors and consequences for water quality. Eur. J. Soil Sci. 58, 523–546.

Köhne, J.M., Köhne, S., Simůnek, J., 2009. A review of model applications for structured soils: a) water flow and tracer transport. J. Contam. Hydrol. 104 (1), 4–35.

Lockwood, P.V., McGarity, J.W., Charley, J.L., 1995. Measurement of chemical weathering rates using natural chloride as a tracer. Geoderma 64 (3), 215–232.

Lorimor, J.C., Mielke, L.N., Elliott, L.F., Ellis, J.R., 1972. Nitrate concentrations in groundwater beneath a beef cattle feedlot. Water Resour. Bull. Am. Water Resour. Assoc. 8 (5), 999–1005.

Mantovi, P., Fumagalli, L., Beretta, G.P., Guermandi, M., 2006. Nitrate leaching through the unsaturated zone following pig slurry applications. J. Hydrol. 316 (1), 195–212.

McCann, I.R., Kincaid, D.C., Wang, D., 1992. Operational characteristics of the watermark model 200 soil water potential sensor for irrigation management. Appl. Eng. Agric. 8 (5), 603–609.

Mielke, L.N., Ellis, J.R., Swanson, N.P., Lorimor, J.C., McCalla, T.M., 1970. Groundwater quality and fluctuation in a shallow unconfined aquifer under a level feedlot. Relationship of agriculture to soil and water pollution. Proceedings, Cornell University Conference on Agricultural Waste Management, Rochester, N.Y., 19 to 21 January 1970, pp. 31–40.

Mielke, L.N., Swanson, N.P., McCalla, T.M., 1974. Soil profile conditions of cattle feedlots. J. Environ. Qual. 3 (1), 14–17.

Miller, J.J., Curtis, T., Larney, F.J., McAllister, T.A., Olson, B.M., 2008. Physical and chemical properties of feedlot pen surfaces located on moderately coarse– and moderately fine–textured soils in Southern Alberta. J. Environ. Qual. 37 (4), 1589–1598.

Olson, B.M., Miller, J.J., Rodvang, S.J., Yanke, L.J., 2005. Soil and groundwater quality under a cattle feedlot in southern Alberta. Water Qual. Res. J. Can. 40 (2), 131–144.

Parker, D.B., Rogers, W.J., McCullough, M.C., Cahoon, J.E., Rhoades, M.B., Robinson, C., 2001. Infiltration characteristics of cracked clay soils in

bottoms of feedyard playa catchments. ASAE Annual International Meeting, Sacramento, CA. vol. 29.
Pengue, W.A., 2005. Transgenic crops in Argentina: the ecological and social debt. Bull. Sci. Technol. Soc. 25 (4), 1–9. http://dx.doi.org/10.1177/0270467605277290.
Pratt, P.F., Lund, L.J., Rible, J.M., 1978. An approach to measuring leaching of nitrate from freely drained irrigated land. In: Nielsen, D.R., et al. (Eds.), Nitrogen in the Environment. Academic Press, New York, pp. 223–273.
Reynolds, W.D., Gregorich, E.G., Curnoe, W.E., 1995. Characterization of water transmission properties in tilled and untilled soils using tension infiltrometers. Soil Till. Res. 33, 117–131.
Rowell, D.L., Martin, M.W., Nye, P.H., 1967. The measurement and mechanism of ion diffusion in soils. III. The effect of moisture content and soil-solution concentration on the self-diffusion of ions in soils. J. Soil Sci. 18, 204–222.
Schaap, M.G., Leij, F.J., 1998a. Using Neural Networks to predict soil water retention and soil hydraulic conductivity. Soil Tillage Res. 47, 37–42.
Schaap, M.G., Leij, F.J., 1998b. Database Related Accuracy and Uncertainty of Pedotransfer Functions. Soil Sci. 163, 765–779.
Schaap, M.G., Leij, F.J., van Genuchten, M.T., 2001. Rosetta: a computer program for estimating soil hydraulic parameters with hierarchical pedotransfer functions. J. Hydrol. 251 (3), 163–176.
Simůnek, J., Jarvis, N.J., van Genuchten, M.T., Gardenas, A., 2003. Review and comparison of models for describing non-equilibrium and preferential flow and transport in the vadose zone. J. Hydrol. 272 (1), 14–35.
Šimůnek, J., van Genuchten, M.T., Šejna, M., 2008. Development and applications of the HYDRUS and STANMOD software packages and related codes. Vadose Zone J. 7 (2), 587–600.
Smith, S.J., Mathers, A.C., Stewart, B.A., 1980. Distribution of nitrogen forms in soil receiving cattle feedlot waste. J. Environ. Qual. 9 (2), 215–218.
Smith, K.A., Jackson, D.R., Withers, P.J.A., 2001. Nutrient losses by surface run-off following the application of organic manures to arable land. 2. Phosphorus. Environ. Pollut. 112 (1), 53–60.
Steinfeld, H., Gerber, P., Wassenaar, T.D., Castel, V., de Haan, C., 2006. Livestock's Long Shadow: Environmental Issues and Options. Food & Agriculture Org.
Stewart, B.A., Viets, F.G., Hutchinson, G.L., Kemper, W.D., Clark, F.E., Fairbourn, M.L., Strauch, F., 1967. Distribution of Nitrates and Other Water Pollutants Under Fields and Corrals in the Middle South Platte Valley of Colorado.
Vaillant, G.C., Pierzynski, G.M., Ham, J.M., DeRouchey, J., 2009. Nutrient accumulation below cattle feedlot pens in Kansas. J. Environ. Qual. 38 (3), 909–918.
van Dam, J.C., Hendrickx, J.M.H., Van Ommen, H.C., Bannink, M.H., van Genuchten, M.T., Dekker, L.W., 1990. Water and solute movement in a coarse-textured water-repellent field soil. J. Hydrol. 120 (1), 359–379.
van Genuchten, M.T., 1980. A closed-form equation for predicting the hydraulic conductivity of unsaturated soils. Soil Sci. Soc. Am. J. 44 (5), 892–898.
van Genuchten, M.T., Nielsen, D.R., 1985. On describing and predicting the hydraulic properties of unsaturated soils. Ann. Geophys. 3 (5), 615–628.
van Genuchten, M.T., Wierenga, P.J., 1976. Mass transfer studies in sorbing porous media I. Analytical solutions. Soil Sci. Soc. Am. J. 40 (4), 473–480.
van Rees, K.C., Sudicky, E.A., Rao, P.S.C., Reddy, K.R., 1991. Evaluation of laboratory techniques for measuring diffusion coefficients in sediments. Environ. Sci. Technol. 25 (9), 1605–1611.
Veizaga, E.A., 2015. Estudio de la dinámica del nitrato en el suelo proveniente de la actividad ganadera intensiva (PhD Thesis) Universidad Nacional del Litoral, Santa Fe, Argentina.
Ventrella, D., Mohanty, B.P., Simůnek, J., Losavio, N., van Genuchten, M.T., 2000. Water and chloride transport in a fine-textured soil: field experiments and modeling. Soil Sci. 165 (8), 624–631.
Wyngaard, N., Videla, C., Picone, L., Zamuner, E., Maceira, N., 2012. Nitrogen dynamics in a feedlot soil. J. Soil Sci. Plant Nutr. 12 (3), 563–574.
Zheng, C., Bennett, G.D., 2002. Applied Contaminant Transport Modeling vol. 2. Wiley-Interscience, New York.